Available online at www.sciencerepository.org

Science Repository

Research Article

Characterization of a Novel Mouse Model of Spontaneous Human Lung Cancer Metastasis

Dongsheng Wang[1], Guoqing Qian[1], Susan Müller[2], Sreenivas Nannapaneni[1], Dong M Shin[1], Nabil F Saba[1] and Zhuo G Chen[1]*

[1]Department of Hematology and Medical Oncology, Winship Cancer Institute, Emory University School of Medicine, Atlanta, GA
[2]Department of Pathology, Emory University School of Medicine, Atlanta, GA

ARTICLEINFO

Article history:
Received: 10 October, 2019
Accepted: 29 October, 2019
Published: 25 November, 2019

Keywords:
Human lung cancer
metastasis
spontaneous metastasis
mouse model
proteomics

ABSTRACT

To identify new strategies against lung metastasis and understand the underlying mechanisms, a highly metastatic pulmonary large cell carcinoma cell line model (801BL) was established through two rounds of *in vivo* selection using a nude mouse xenograft model. Satellite tandem repeat (STR) analysis confirmed the same genomic background of the newly established metastatic cell line 801BL as the non-metastatic 801C and low-metastatic 801D counterparts. Our study showed that 100% of mice (8 out of 8) injected subcutaneously with 801BL cells developed lung metastatic tumors, while none of the mice injected with 801C cells had lung metastasis ($p<0.0001$). Highly metastatic 801BL cells showed alterations in morphology and invasion capability when compared with 801C and/or 801D cell lines A comparative proteomic analysis between 801BL and 801C followed by bioinformatics analysis revealed significant alterations in several dominant cell signalling networks in the highly metastatic cell line. Western blot confirmed the proteomic findings for several proteins from each signalling network. Since the highly metastatic cell line and its non-metastatic counterpart share the identical genetic background, this model provides a powerful tool for study of the mechanisms underlying lung cancer metastasis.

Introduction

Lung cancer is the deadliest type of cancer for both men and women. It is estimated that 234,030 new cases of lung cancer will be diagnosed in 2018 and 154,050 deaths are projected in the United States, where 90% of cancer deaths can be attributed to metastasis [1, 2]. The underlying mechanisms of metastasis in most cancers including lung cancer are still poorly understood.

Metastasis studies require both pathologic and *in vivo* animal analyses, because metastasis is a biological process with multiple steps that can only be described based on *in vivo* analysis. Without animal studies, there is high potential for misinterpretation [3]. Preclinical animal tumor models are a fundamental component of the study of metastatic cancer. Several types of animal models have been developed for experimental lung cancer research including chemically induced lung tumors, human tumor xenografts, and transgenic mouse models [4]. Among these models, xenografts are reliable tools for the study of metastatic disease mainly because other models generally produce a low incidence of distant metastatic disease [5].

To understand the underlying mechanisms of metastasis, it is crucial to understand the molecular profiles of the metastatic cancer cells at transcriptional and translational levels. Recent data show, however, that human neoplasms are biologically heterogeneous and that the process of clinical metastasis is selective [6-8]. Transcriptional profile analysis of tumor tissue revealed critical pathways associated with effects on tumor-host interaction and inhibition of tumor growth. Studies using *in situ* hybridization and immunohistochemical staining have shown that the expression of genes and/or proteins associated with proliferation, angiogenesis, cohesion, motility, and invasion vary among different regions of neoplasms [9, 10]. Because of the heterogeneity of tumor cells and the tumor infiltration by normal host cells and non-metastatic tumor cells, the search for genes and/or proteins that are associated with

**Correspondence to: Zhuo G Chen, Department of Hematology and Medical Oncology, Winship Cancer Institute, Emory University School of Medicine, 1365-C Clifton Road, Suite C3086, Atlanta, GA 30322; Tel: 404-778-3977; Fax: 404-778-5520; E-mail: gzchen@emory.edu*

http://dx.doi.org/10.31487/j.COR.2019.5.13

metastasis cannot be conducted appropriately by the indiscriminate and nonselective analysis of tumor tissues [3]. Therefore, metastatic cell lines, ideally isogenic cell lines derived from their non-metastatic parental cells, have become essential biological materials for this type of study.

It is critical to improve our understanding of the characteristics of metastatic cells, which will allow us to target this disease for therapeutic intervention. Clearly, the pathogenesis of metastasis depends on multiple interactions between metastatic cancer cells and host homeostatic mechanisms. In this study, we established a novel metastatic lung cancer model through *in vivo* selection and compared phenotype and proteomic profiles between the metastatic cells and their non-metastatic counterparts. We hope this study can provide a valuable tool to understand how cancer cells become metastatic

Materials and Methods

I Cell lines and culture

Large cell lung cancer cell lines PLA-801C and PLA-801D were obtained from Dr. Y.L. Lu (Institute of Basic Medical Science, China). 801C and 801D are non-metastatic and low metastatic cell clones, respectively, from the same cell line PLA-801 [11]. All cell lines including the newly established 801BL cells were cultured in RPMI 1640 medium with 10% FBS at 37 °C. For suspension culture, cells were seeded in a 1.25% poly-hydroxyethyethylmethacrylate (Millipore Sigma Co. St. Louis, MO) treated tissue culture dish for 96 h. The cell viability was determined using flow cytometry. For apoptosis assay, cell spheroids were collected and digested with 0.25% trypsin. PE Annexin V Apoptosis Detection Kit (BD Biosciences, San Jose, CA) was used according to manufacturer's instructions.

II Cell invasion assay

The matrigel invasion assay was performed using the matrigel basement membrane matrix according to the manufacturer's protocol (Becton Dickinson Biosciences Discovery Labware, Bedford, MA). Briefly, 3×10^4 cells in 0.5 mL of serum-free medium were seeded in the invasion chamber containing the matrigel membrane (27.2 ng per chamber) in triplicate and allowed to settle for 3 hours at 37 °C. NIH3T3-conditioned medium was added as a chemoattractant in the lower compartment of the invasion chamber. The chambers were incubated for 24 hours at 37 °C in a 5% CO2 atmosphere. The invading cells appeared at the lower surface of the membrane. The upper surface of the membrane was scrubbed with a cotton swab and the absence of cells in the upper surface was confirmed under the light microscope. After the cells were fixed and stained with crystal violet, the membrane was placed on a microscope slide with the bottom side up and covered with immersion oil and a cover slip. Cells were counted under a microscope as a sum of 10 high power fields that were distributed randomly on the central membrane. The experiment was repeated 3 times.

III Stable isotope labeling by amino acids in cell culture (SILAC)

Proteomics samples were prepared using Pierce SILAC protein quantitation kit following the manufacturer's instructions (Thermo Scientific, Waltham, MA). Stable amino acids were purchase from Cambridge Isotope Laboratories, Inc (Andover, MA). Protein profiling study by isotopic labeling mass spectrometry analysis was conducted by the Center of Functional Genomics at the University of Albany-SUNY.

IV Western-blot assay

Cells were washed twice with PBS before being lysed on ice for 30min with lysis buffer containing 50mmol/L HEPES buffer, 150mmol/L NaCl, 1mmol/L EDTA (pH 8.0), 1mmol/L EGTA (pH8.0), 1% IGEPAL CA-630, 0.5% Triton X-100, 10mmol/L NaF, 2mmol/L Na3VO4, 10mmol/L β-glycerophosphate and 1% Protease Inhibitor Cocktail (Sigma-Aldrich, St Louis, MO). The lysate was centrifuged at 16,000 g at 4°C for 15 min. 50 micrograms of total protein for each sample were separated by 10% SDS-PAGE and transferred onto a Westran S membrane (Whatman Inc. Floham Park, NJ), and desired proteins were probed with corresponding antibodies. Mouse anti-LDHA was purchased from LifeSpan BioScience Inc.; mouse anti-human actin (1:100 dilution) from Milipore Sigma; mouse anti-human E-cadherin antibody was purchased from BD Bioscience; rabbit anti–human ezrin antibody was purchased from Cell Signaling; mouse anti-vinculin and sheep anti-TGM 2 antibodies were purchased from R&D Systems. Bound antibody was detected using the SuperSignal West Pico Chemoluminescence system (Pierce, Inc., Rockford, IL).

V Satellite tandem repeat (STR) analysis

A PCR based microsatellite marker analysis was performed in the Research Animal Diagnostic Laboratory (Radil Lab, Missouri University) to confirm cell originality. Nine microsatellite markers were evaluated.

VI Xenograft metastasis mouse model

Animal experiments were approved by the Institutional Animal Care and Use Committee (IACUC) of Emory University and followed the IACUC guidelines. In brief, nude mice (athymic nu/nu, Taconic, NY, USA) aged 4–6 weeks (about 20 g bodyweight) were randomly divided into two groups. 801C cells (2×10^6) suspended in 0.10 ml of Hanks-buffered saline was injected subcutaneously into flank of group 1 mice. Each animal in group 2 was injected with 2×10^6 801BL cells. Xenograft tumors were measured three times per week. Mice were euthanized 4-6 weeks after the initial injection; animal lungs were collected, fixed immediately in 10% buffered formalin, and embedded in paraffin. Tissue sections were stained with hematoxylin–eosin (H&E). Five sections were made for each sample. Lymph node and lung metastases were identified by two individuals (SM and DW).

Results

I Establishing highly metastatic 801BL cells through in vivo selection

Two rounds of *in vivo* selection using a nude mouse xenograft model were used to generate a highly metastatic cell line. In the first round, low-metastatic human large cell lung cancer cells 801D (2×10^6) were subcutaneously injected into the flank of 6 nude mice. After 6 weeks, the

mice were sacrificed, and brain and lung tissue and were cut into small fragments of <1mm^3. Fragments were subjected to 0.25% trypsin digestion for 30 min, isolated cells (very few, the pellet was barely visible) were washed and cultured in RPMI medium. Colonies of cancer cells were found in brain tissue culture in only 1 out of 6 mice. After expanding *in vitro* for 3 passages, the cells were collected and subjected to another round of subcutaneous injection. After another 8 weeks, metastatic nodules were found in the lung. The nodules were harvested and cut into small fragments which were then disassociated with 1% collagenase (Millipore Sigma) in a gently shaking water bath for 1 h at 37 °C. After passing through an 85 μm mesh sieve, the resulting cell suspension was washed twice and centrifuged at a speed of 300 g ×15 min. The pellet was then washed and cultured in RPMI 1640 medium. A highly metastatic cell line, 801BL, was established from the lung metastatic cells. A PCR-based satellite tandem repeat (STR) analysis confirmed that the genomic background of the newly established metastatic cell line 801BL was the same as that of the non-metastatic counterpart 801C and low-metastatic counterpart 801D (Table 1). Since 801C and 801D cells are morphologically almost identical, in the majority of our study, the newly established cell line 801BL was examined for its metastatic ability compared to the non-metastatic 801C cell line only.

Marker Name	Cell Lines		
	801 C	801 D	801 BL
Amelogenin	**X, Y**	**X, Y**	**X, Y**
CSF1PO	12	12	12
D13S317	12	12	12
D16S539	13	13	13
D5S818	11	11	11
D7S820	9	9	9
TH01	7	7	7
TPOX	9, 11	9, 11	9, 11
vWA	18	18	18

Table 1: Satellite tandem repeat (STR) analysis confirms the same genomic background of 801BL, 801C and 801D cell lines.

II 801BL cells but not 801C cells developed lung metastasis after subcutaneous injection in the flank of mice

To determine the metastatic potential of the newly established cell line, 801BL cells were injected subcutaneously into the flank of nude mice. Animals were sacrificed 6 weeks after and lung samples were collected for H&E staining. The same experiments were conducted on 801C and 801D cells as control. None of the mice injected with 801C cells developed lung metastasis, while all 8 mice in the 801BL-injected group showed lung metastasis. Some of the metastatic tumors in the lung could even be visually observed (Figure 1). Metastasis was found in only 1 mouse among the 8 mice injected with 801 D cells.

III 801BL cells exhibit different morphological characteristics from 801C cells

801BL cells present pluripotent cell-like morphological changes compared to 801C cells and display a rounded shaped with de-differentiated morphological characteristics in *in vitro* culture. 801BL cells grow like semi-adherent cells especially in the first 48 h after seeding and are slower to attach to the culture flask compared to 801C cells. 801BL cells are also smaller than 801C cells. Representative microscopic images of 801C cell and 801BL cells were taken 24, 48, and 72 hours after cells were seeded (Figure 2).

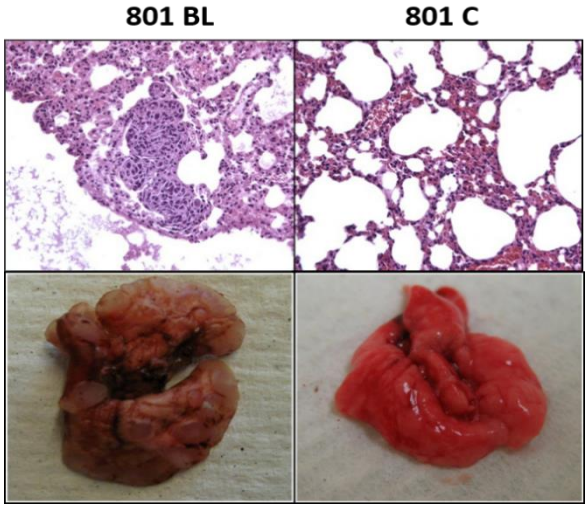

Cell Type	Number of Mice	Number of Lung Met
801C	**8**	**0**
801D	**8**	**1**
801 BL	**8**	**8**

Figure 1: Only 801BL cells generate metastasis in a xenograft animal model. 801C, 801D and 801BL cells were injected subcutaneously into the flank of nude mice. Animals were sacrificed after 4 weeks. Animal lung samples were collected for H&E staining (A). None of the mice injected with 801C cells had lung metastasis, while all mice in the 801BL cells group showed lung metastasis (B). Some of the metastatic tumors in the lung could even be visually observed (A). (Image represents 1 in 8 mice from each group).

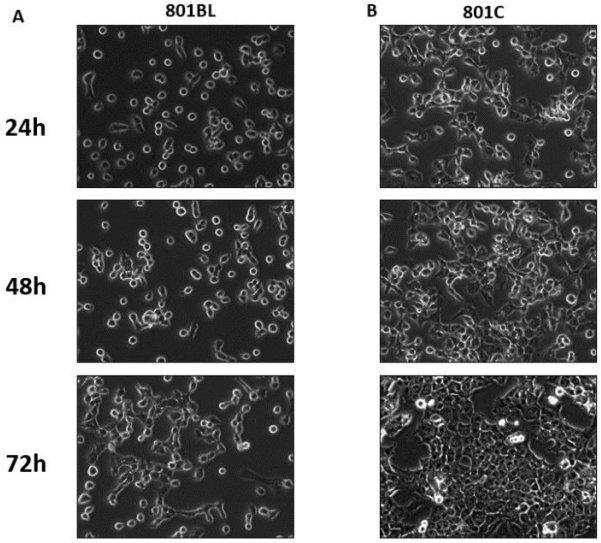

Figure 2: 801BL cells have pluripotent cell features. After a 2-round *in vivo* selection, 801BL cells (A) exhibit pluripotent cell-like morphological change compared to 801 C cells (B). 801BL cells display a rounded-shaped and appear de-differentiated in *in vitro* culture. 801BL cells are also smaller than 801C cells. Image shows representative microscopic images of 801C and 801BL cells at 24, 48 and 72 hs.

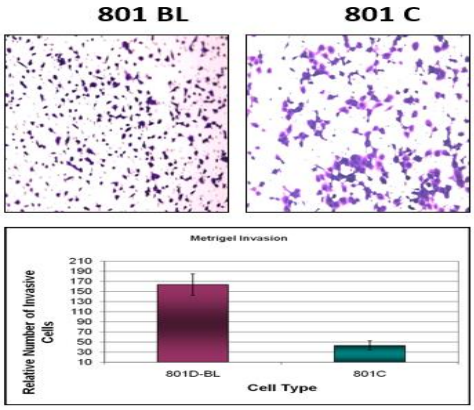

Figure 3: 801BL cells are more invasive than 801C cells. 801C and 801BL cells were seeded at 3×10^4 cells per chamber containing the matrigel membrane. A matrigel invasion assay was performed after 24 h. Invasive cells were counted as a sum of 10 high power fields (×200) in the central membrane under the microscope. The invasive capability of 801BL cells was increased by 3.47±0.44-fold compared to the non-metastatic counterpart 801C cells ($p<0.001$). Matrigel invasion assay for each cell line was repeated 3 times.

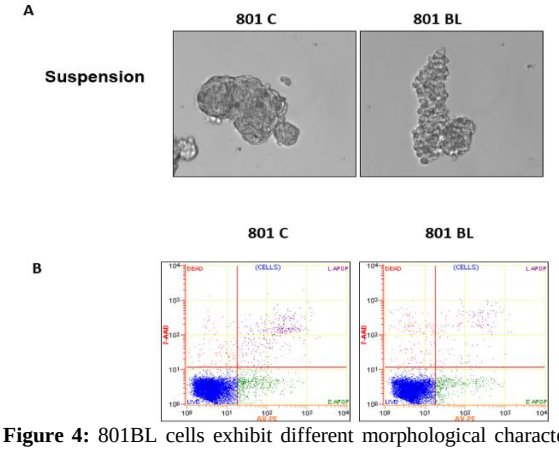

Figure 4: 801BL cells exhibit different morphological characteristics from 801C cells. Cells were seeded in a 1.25% poly-hydroxyethyethylmethacrylate (Sigma) treated tissue culture dish for 96 h. (A) shows that spheroids from 801BL cells looked different under the microscope (100×) than those from 801C cells. Single cells were still visible for 801BL cells while the cell boundary was difficult to distinguish for 801C cells. (B) 801BL cells showed better survival in suspension culture conditions than 801C cells, with a cell death rate of 6.21% compared to 11.3% for 801C cells. The assay was repeated 3 times.

IV 801BL cells are more invasive than 801C cells

Since 801BL cells display some pluripotent morphological changes compared to 801C cells, and because invasion and migration are the two most prominent features of metastatic cells, we analyzed the invasion activity of 801C and 801BL cells. Cells were seeded in matrigel coated chambers. After 24 h, invasive cells were counted as a sum of 10 high power fields (×200) in the central membrane under the microscope. The invasive capability of 801BL cells was increased by 3.47±0.44-fold compared to the non-metastatic counterpart 801C cells ($p<0.001$). The matrigel invasion assay for each cell line was repeated 3 times (Figure 3). No significant difference in migration of the two cell lines was found (data not shown).

V 801BL cells survive suspension culture condition

801BL and 801C cells were seeded in poly-HEMA treated tissue culture dishes and cultured for 96 h. Cell viability was determined by flow cytometry assay. As shown in (Figure 4), the spheroids from 801BL cells looked different from 801C cells. Single cells were visible for the 801 BL cell line, while the cell boundary was difficult to distinguish for 801C cells. 801BL cells survived better in suspension culture condition, with a cell death rate of 6.21% compared to 11.3% for 801C cells ($p<0.05$).

Genes Increased in 801BL Cells **5A**

Fold Change	ID	Symbol	Entrez Gene Name
9999.000	IPI00791086.2	EIF3D	eukaryotic translation initiation factor 3, subunit D
9999.000	IPI00956400.1	BBS1	Bardet-Biedl syndrome 1
9999.000	IPI00607732.1	NCLN	nicalin
9999.000	IPI00908752.1	CMPK1	cytidine monophosphate (UMP-CMP) kinase 1, cytosolic
28.424	IPI00554648.3	KRT8	keratin 8
10.080	IPI00554788.5	KRT18	keratin 18
6.442	IPI00924788.2	NCEH1	neutral cholesterol ester hydrolase 1
4.121	IPI00872684.1	EZR	ezrin
3.754	IPI00007321.2	LYPLA1	lysophospholipase I
3.399	IPI00031169.1	RAB2A	RAB2A, member RAS oncogene family
3.339	IPI00003505.3	TRIP13	thyroid hormone receptor interactor 13
3.338	IPI00294578.1	TGM2	transglutaminase 2 (C polypeptide, protein-glutamine-gamma-glutamyltransferase)
3.198	IPI00307162.2	VCL	vinculin
3.034	IPI00218918.5	ANXA1	annexin A1
2.883	IPI00747810.2	FSCN1	fascin homolog 1, actin-bundling protein (Strongylocentrotus purpuratus)
2.412	IPI00003856.1	ATP6V1E1	ATPase, H+ transporting, lysosomal 31kDa, V1 subunit E1
2.363	IPI00418169.3	ANXA2	annexin A2
2.293	IPI00221222.7	SUB1	SUB1 homolog (S. cerevisiae)
2.248	IPI00872814.1	MSN	moesin
2.197	IPI00032304.2	PLS1	plastin 1
2.063	IPI00007752.1	TUBB4B	tubulin, beta 4B class IVb
1.980	IPI00007694.5	PPME1	protein phosphatase methylesterase 1
1.946	IPI00964364.1	EEF1E1	eukaryotic translation elongation factor 1 epsilon 1
1.892	IPI00938079.1	PDCD6IP	programmed cell death 6 interacting protein
1.881	IPI00026216.4	NPEPPS	aminopeptidase puromycin sensitive
1.877	IPI00815642.1	TMSB10/TMSB4X	thymosin beta 10
1.866	IPI00479186.7	PKM	pyruvate kinase, muscle
1.847	IPI00947127.1	LDHA	lactate dehydrogenase A
1.832	IPI00010080.2	OXSR1	oxidative-stress responsive 1
1.816	IPI00219219.3	LGALS1	lectin, galactoside-binding, soluble, 1
1.811	IPI00604710.2	SLC3A2	solute carrier family 3 (activators of dibasic and neutral amino acid transport), member 2
1.787	IPI00006666.1	SLC16A3	solute carrier family 16, member 3 (monocarboxylic acid transporter 4)
1.763	IPI00556308.4	GYG1	glycogenin 1
1.761	IPI00878984.1	DDT	D-dopachrome tautomerase

Genes Decreased in 801BL Cells **5B**

Fold Change	ID	Symbol	Entrez Gene Name
-1.754	IPI00395627.3	CACYBP	calcyclin binding protein
-1.755	IPI00007765.5	HSPA9	heat shock 70kDa protein 9 (mortalin)
-1.768	IPI00221108.5	TYMS	thymidylate synthetase
-1.773	IPI00010415.2	ACOT7	acyl-CoA thioesterase 7
-1.779	IPI00020127.1	RPA1	replication protein A1, 70kDa
-1.837	IPI00794221.1	DBN1	drebrin 1
-1.840	IPI00930710.1	SLC25A13	solute carrier family 25 (aspartate/glutamate carrier), member 13
-1.868	IPI00220834.8	XRCC5	X-ray repair complementing defective repair (double-strand-break rejoining)
-1.898	IPI00217467.3	HIST1H1E	histone cluster 1, H1e
-1.922	IPI00009790.1	PFKP	phosphofructokinase, platelet
-1.929	IPI00909207.1	PRDX2	peroxiredoxin 2
-1.964	IPI00514587.1	SARS	seryl-tRNA synthetase
-1.976	IPI00419373.1	HNRNPA3	heterogeneous nuclear ribonucleoprotein A3
-2.032	IPI00220362.5	HSPE1	heat shock 10kDa protein 1 (chaperonin 10)
-2.065	IPI00289499.3	ATIC	5-aminoimidazole-4-carboxamide ribonucleotide formyltransferase/IMP cyclohydrolase
-2.069	IPI00784154.1	HSPD1	heat shock 60kDa protein 1 (chaperonin)
-2.069	IPI00942520.1	PRMT1	protein arginine methyltransferase 1
-2.121	IPI00026833.4	ADSS	adenylosuccinate synthase
-2.238	IPI00009210.1	DUSP12	dual specificity phosphatase 12
-2.293	IPI00843789.2	GLDC	glycine dehydrogenase (decarboxylating)
-2.773	IPI00967299.1	PARP1	poly (ADP-ribose) polymerase 1
-2.825	IPI00020418.1	RRAS	related RAS viral (r-ras) oncogene homolog
-2.886	IPI00011200.5	PHGDH	phosphoglycerate dehydrogenase
-2.921	IPI00059135.1	PPP1R14A	protein phosphatase 1, regulatory (inhibitor) subunit 14A
-3.632	IPI00930174.1	HIST2H2BF	histone cluster 2, H2bf
-3.989	IPI00219037.5	H2AFX	H2A histone family, member X
-4.444	IPI00515061.3	HIST1H2BJ/HIST1H2BK	histone cluster 1, H2bk

Figure 5: Proteomics study shows that 801BL cells exhibit a different protein profile from 801C cells. Some proteins were expressed at a higher level in 801BL than 801C cells (A), while others were expressed at a lower level (B) (cut-off threshold is 1.75-fold change).

VI Proteomics study shows 801BL cells display a different protein profile to 801C cells

Samples for proteomics analysis were prepared using Pierce SILAC protein quantitation kit. Isotopic stable amino acid labeled 801BL cell lysate mixed with non-labeled 801C cell lysate was subjected to mass spectrometry analysis (Supplementary Figure S1). Proteomics study showed 801BL cells displayed a different protein profile compared to

801C cells (Figure 5A and 5B). Bioinformatics analysis revealed significant alterations in several dominant cell signaling networks between these two cell lines, including those involved in cell morphology, cellular function and maintenance, DNA replication, recombination, and repair, and cell death (Supplementary Figure S2).

VII Proteomics analysis findings were confirmed by Western blot assay

To confirm the findings from proteomics analysis, several proteins from each altered cell signaling network were chosen for immunoblot study. As shown in (Figure 6A), protein alterations found in the proteomics study [lactate dehydrogenase A (LDHA), ezrin, RAB-2A, vinculin, transglutaminase 2 (TGM2)] were confirmed by Western blot: the levels of LDHA (cellular function and maintenance), ezrin and vinculin (cell morphology), RAB-2A (cell death), and TGM2 (DNA repair, replication, recombination) were all increased in both 801D and 801BL cells compared to 801C cells, and vinculin expression was higher in 801BL than in 801D cells. Although not detected in the proteomics assay, the expression levels of metastasis-related genes E-cadherin and Twist were also determined by Western blot assay and were found to be lower and higher, respectively, in 801BL cells compared to 801C cells (Figure 6 B).

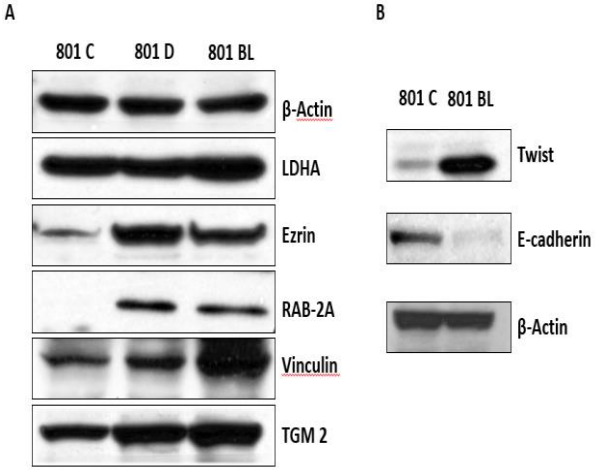

Figure 6: Western blot assay confirms proteomics findings A, several proteins from each altered cell signaling network were chosen for immunoblot study. Alterations found in the proteomics study in the expression of proteins (LDHA, ezrin, RAB-2A, vinculin, TGM2) were confirmed by Western blot. B. Metastasis-related genes Twist and E-cadherin were also found to be expressed differently between 801C and 801BL cells.

Discussion

Metastasis is the hallmark of malignant tumors and the primary cause of cancer patient death [2]. Therefore, better understanding of the molecular mechanisms underlying the metastasis of cancer and the identification of predictive metastatic and prognostic markers will contribute significantly to our ability to predict and guide the treatment of this disease. An *in vivo* system that incorporates the features of metastatic tumor and models the dynamic response to cancer drug treatment may facilitate the development of precision medicine targeting metastasis. In this study, we used two rounds of *in vivo* selection to establish a highly metastatic cell line which can metastasize to lung spontaneously after subcutaneous inoculation. By analyzing the biological differences between this highly metastatic cell line and its non-metastatic counterpart, we are able to identify some molecular events that are unique in metastasis. We believe this new lung metastasis model could provide us a useful tool to study cancer metastasis.

Our model is a spontaneous xenograft model. Several metastasis models are currently employed that fall into two categories, spontaneous and experimental metastasis models. Spontaneous models include allograft, xenograft and patient-derived xenograft (PDX) models [12]. Each model has its own advantages and shortcomings in terms of mimicking the actual biological process of human cancer metastasis. The metastatic capacity of cancer cells is determined by genetic and epigenetic changes within the tumor as well as contributions from the tumor microenvironment (TME) [13, 14]. We used the *in vivo-in vitro* method to isolate metastatic cancer cells. It has been shown that the increase in metastatic capacity using this approach does not result from adaption of tumor cells to preferential growth in a specific organ or environment but, rather, is due to the selection [15-17]. This procedure was originally used to isolate the B16-F10 line from wild-type B16 melanoma, but has also been successfully used to produce highly metastatic tumor cell lines from many murine and human tumors [18, 19]. It is worth pointing out that in the first round of selection, metastatic cells were selected from the mouse brain. We did not successfully isolate metastatic cells in the lung from the same animal. This could be due to the complex and highly heterogeneous mixture of the lung tissue which results in difficulty in isolating a relatively small number of cancer cells. In the second round of *in vivo* selection, the cell line formed large masses of lung metastasis which could be visually identified and consisted mostly of cancer cells; therefore, the final metastatic cell line was isolated from lung.

Our selected cells have several metastasis signatures that help them achieve metastasis. The process of metastasis is a multistep cascade that results from the accumulation of multiple genetic and epigenetic alterations [3, 20, 21]. It has been shown that carcinoma cells first invade the surrounding stroma, then migrate and intravasate into the blood or lymphatic vessels and survive anoikis. Once arrested in the capillaries of a distant location or organ, they will penetrate the adjacent parenchyma, and adapt to the newly colonized site or subvert the local microenvironment to form the new tumor. Only cells with metastatic features can fulfil all these steps and achieve metastasis. First, as our invasion assay study (Figure 3) has shown, the highly metastatic cells are more invasive than their non-metastatic counterpart. This is expected since invasion is fundamental for the first step of cancer cells leaving the primary site. This feature helps the cells break through the extracellular matrix (ECM) to fulfill the mission of intravasation, extravasation, and reaching the metastatic site. Second, the selected 801BL cells survive better under non-attached conditions (Fig 4). For tumor cells to establish new colonies growing in a distant location, they have to survive lengthy travel within the blood flow. This feature helps the cells overcome anoikis in the blood. Finally, the epithelial-mesenchymal transition (EMT) feature of our selected cell line provides the biological mechanism underlying metastasis. Our morphological examination and Western blot results showed 801BL cells are EMT-like (Figure 2) and have reduced expression of E-cadherin and higher expression of

TWIST1 (Figure 6), which are hallmarks of EMT cells, as compared with the non-metastatic counterpart. EMT plays a major role in embryogenesis, organ development and tissue regeneration [22]. Recently, EMT has been demonstrated to be highly associated with cancer progression and metastasis [23, 24]. It is worth pointing out that EMT is hypothesized to be an absolute requirement for tumor invasion and metastasis interaction. Its reverse process, mesenchymal-epithelial transition (MET), is also essential for metastasis because cancer cells need to undergo the reverse of EMT once they reach the metastasis site and begin colonization and growth [25, 26]. Although we observed EMT in the 801BL line compared to its non-metastatic counterpart, we do not know if 801 BL cells will undergo MET changes at the metastatic site since we cannot mimic the MET process *in vitro*.

Using our current model, we identified several potentials signaling pathways that could be targeted in the treatment of metastasis. To identify biomarkers and signaling pathways in metastatic cancer cells, we performed a proteomics study. Some specific proteins were identified to have a different expression pattern in the two cell lines (Figure 5A and 5B). To confirm the validity of the proteomics assay, we performed Western blot assays on selected proteins that showed different expression in the proteomics assay (Figure 6). Of the tested proteins, vinculin is associated with focal adhesion and adherens junctions, which are complexes that nucleate actin filaments and crosslinkers between the external medium, plasma membrane, and actin cytoskeleton; LDHA has been shown to play an important role in the development, invasion and metastasis of malignancies; TGM2 displays several intra- and extracellular activities in relation to cell death, survival and differentiation; ezrin plays a key role in cell surface structure adhesion, migration, and organization [27-30]. All Western blot results confirmed the accuracy of the proteomics findings. These data provide some clues and potential targets for treating or preventing metastasis disease. Several signaling pathways were identified after analysis with Ingenuity IPA software. The major differences between 801BL and 801C cells are in molecular networks that function in cellular assembly and organization, cell cycle, organismal survival, cell-to-cell signaling and interaction, cell death and cell morphology. Considering the large number of differences in protein expression between 801BL and 801C cell lines, it is reasonable to assume that functional molecular networks are also altered between the two cell lines. This finding is not surprising since all of these networks are important for tumor cells to migrate and settle in the new milieu. Our current study focuses on protein expression profile changes in the metastatic cell line compared to its non-metastatic counterpart, because we believe the newly established cell line is the result of the selection of a pre-existing population in the original cells, rather than a selection of an in-process gene mutation that occurred during the two-round selection. We focus on the protein profile of the metastatic cell line also because proteins are the foot soldiers responsible for nearly all biological functions and events within cells. Proteins are also most likely the targets for drugs that treat or prevent metastasis. Nonetheless, it is still of great interest to identify any possible single or multi-genetic differences between the 801BL cells and their non-metastatic counterpart.

As is the case with nearly all metastatic models, our new model may not provide a complete picture of cancer metastasis. Since our model is xenograft-based, the power of this model in determining the effect of TME is certainly limited because of the differences in metastatic organ sites between humans and mice, especially the difference in the immune system between humans and mice. However, our model can still provide valuable genetic and epigenetic information regarding a metastatic cancer.

In conclusion, a highly metastatic cell line was established through two rounds of *in vivo* selection in this study. Since the 801BL cell line has the same genetic background as its non-metastatic counterpart, the difference in their protein expression profile is most likely specific for metastasis; this model will thus provide a new powerful tool to understand the mechanisms underlying cancer metastasis. At the same time, it is an ideal model for testing anti-metastasis agents in the research setting.

Funding

The study was supported by a grant from the Department of Defense: DOD W81XWH-07-1-0306 to Dr. Chen, ZG.

Author Contributions

Conceptualization: D.W. and Z.G.C.; Methodology: D.W., G.Q, S.M., and Z.G.C.; Validation: D.W. and S.M.; Formal analysis: D.W. Investigation and data curation: D.W. and S.N.; Resources: D.M.S and Z.G.C.; Writing-Original draft preparation: D.W.; Writing-review, editing, and supervision: N.F.S. and Z.G.C.; Funding acquisition: Z.G.C.

Acknowledgement

The authors thank Dr. Anthea Hammond for her editing of the manuscript.

Conflict of Interest

The authors declare no conflict of interests.

Supplementary Materials

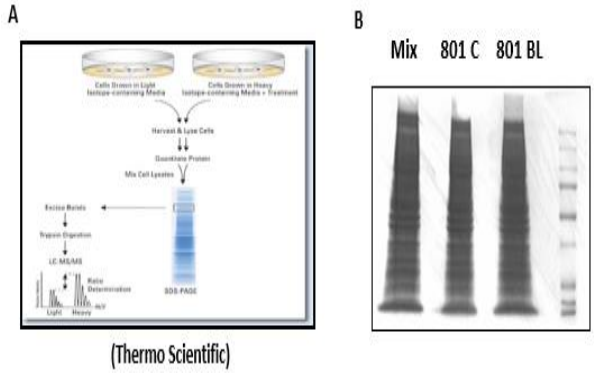

Figure S1: Proteomics samples were prepared using Pierce SILAC protein quantitation kit according to the manufacturer's protocol (A). Lysate from 801BL cells labeled with isotopic stable amino acids was mixed with the same amount of 801C cell lysate. (B) Equal amounts of cell lysates were loaded for SDS-PAGE to ensure comparable protein

quantity for 801BL and 801C cells before sending for mass spectrometry analysis.

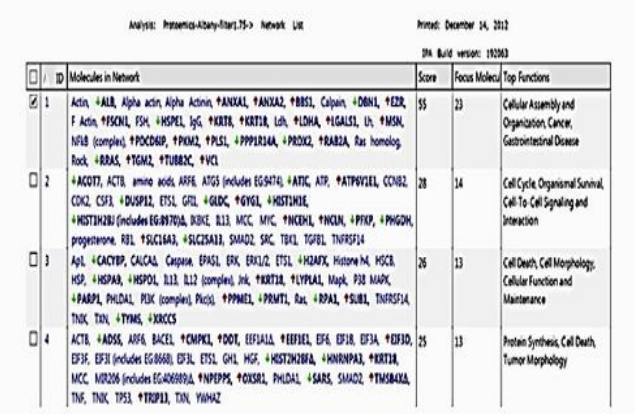

Analysis: Proteomics-Albany-filter1.75-> Network List — Printed: December 14, 2012 — IPA Build version: 192063

ID	Molecules in Network	Score	Focus Molecu	Top Functions
1	Actin, ↑ALB, Alpha actin, Alpha Actinin, ↑ANXA1, ↑ANXA2, ↑BBS1, Calpain, ↓DBN1, ↑EZR, F Actin, ↑FSCN1, FSH, ↓HSPE1, IgG, ↑KRT8, ↑KRT18, Ldh, ↑LDHA, ↑LGALS1, Lh, ↑MSN, NFkB (complex), ↑PDCD6IP, ↑PKM2, ↑PLS1, ↓PPP1R14A, ↓PRDX2, ↑RAB2A, Ras homolog, Rock, ↓RRAS, ↑TGM2, ↑TUBB2C, ↑VCL	55	23	Cellular Assembly and Organization, Cancer, Gastrointestinal Disease
2	↓ACOT7, ACTB, amino acids, ARF6, ATG5 (includes EG:9474), ↓ATIC, ATP, ↑ATP6V1E1, CCNB2, CDK2, CSF3, ↓DUSP12, ETS1, GFI1, ↓GLDC, ↑GYG1, ↓HIST1H1E, ↓HIST2H2BJ (includes EG:89702), IKBKE, IL13, MCC, MYC, ↑NCEH1, ↑NCLN, ↓PFKP, ↓PHGDH, progesterone, RB1, ↑SLC16A3, ↓SLC25A13, SMAD2, SRC, TBX3, TGFB1, TNFRSF14	28	14	Cell Cycle, Organismal Survival, Cell-To-Cell Signaling and Interaction
3	Ap1, ↑CACYBP, CALCA, Caspase, EPAS1, ERK, ERK1/2, ETS1, ↓H2AFX, Histone h4, HSC8, HSP, ↑HSPA8, ↑HSPD1, IL13, IL12 (complex), Jnk, ↑KRT38, ↑LYPLA1, Mapk, P38 MAPK, ↓PARP1, PHLDA1, PI3K (complex), Pkcb, ↑PPME1, ↓PRMT1, Ras, ↓RPA1, ↑SUB1, TNFRSF14, TNIK, TXN, ↓TYMS, ↓XRCC5	26	13	Cell Death, Cell Morphology, Cellular Function and Maintenance
4	ACTB, ↑ADSS, ARF6, BACE1, ↑CMPK1, ↑DDT, EEF1A1L, ↑EEF1E1, EF4, EIF1B, EIF3A, ↑EIF3D, EIF3F, EIF3I (includes EG:8668), EIF3L, ETS1, GH1, HGF, ↓HIST2H2BFA, ↓HNRNPA3, ↑KRT38, MCC, MIR206 (includes EG:406989), ↑NPEPPS, ↑OXSR1, PHLDA1, ↓SARS, SMAD2, ↑TMSB4XA, TNF, TNIK, TP53, ↑TRIP13, TXN, YWHAZ	25	13	Protein Synthesis, Cell Death, Tumor Morphology

Figure S2: Bioinformatics analysis using Ingenuity® Pathway Analysis (IPA®) revealed significant alterations in several dominant cell signaling networks including those involved in cell morphology, cellular function and maintenance, DNA replication, recombination, and repair, and cell death between the two cell lines. (p-value: 1.08E-08-6.83E-03) and cell death (p-value: 1.88E-08-6.83E-03), between the highly metastatic cell line (801BL) and its non-metastatic counterpart (801C)

REFERENCES

1. Siegel RL, Miller KD, Jemal A (2019) Cancer statistics. *CA Cancer J Clin* 69: 7-34. [Crossref]
2. Seyfried TN, Huysentruyt LC (2013) On the origin of cancer metastasis. *Crit Rev Oncog* 18: 43-73. [Crossref]
3. Talmadge JE, Fidler IJ (2010) AACR centennial series: the biology of cancer metastasis: historical perspective. *Cancer Res* 70: 5649-5669. [Crossref]
4. Liu J, Johnston MR (2002) Animal models for studying lung cancer and evaluating novel intervention strategies. *Surg Oncol* 11: 217-227. [Crossref]
5. Francia G, Cruz-Munoz W, Man S, Xu P, Kerbel RS (2011) Mouse models of advanced spontaneous metastasis for experimental therapeutics. *Nat Rev Cancer* 11: 135-141. [Crossref]
6. Fidler IJ (2012) Biological heterogeneity of cancer: implication to therapy. *Hum Vaccin Immunother* 8: 1141-1142. [Crossref]
7. Bissig H, Richter J, Desper R, Meier V, Schraml P et al. (1999) Evaluation of the clonal relationship between primary and metastatic renal cell carcinoma by comparative genomic hybridization. *Am J Pathol* 155: 267-274. [Crossref]
8. Kuukasjarvi T, Karhu R, Tanner M, Kahkonen M, Schaffer A et al. (1997) Genetic heterogeneity and clonal evolution underlying development of asynchronous metastasis in human breast cancer. *Cancer Res* 57: 1597-1604. [Crossref]
9. Fidler IJ (2002) Critical determinants of metastasis. *Semin Cancer Biol* 12: 89-96. [Crossref]
10. Simone NL, Bonner RF, Gillespie JW, Emmert-Buck MR, Liotta LA (1998) Laser-capture microdissection: opening the microscopic frontier to molecular analysis. *Trends Genet* 14: 272-276. [Crossref]
11. Lu YL (1989) Spontaneous metastasis of clonal cell subpopulations of human lung giant cell carcinoma after subcutaneous inoculation in nude mice. *Zhonghua Zhong Liu Za Zhi* 11: 1-7. [Crossref]
12. Gomez-Cuadrado L, Tracey N, Ma R, Qian B, Brunton VG (2017) Mouse models of metastasis: progress and prospects. *Dis Model Mech* 10: 1061-1074. [Crossref]
13. DeClerck YA, Pienta KJ, Woodhouse EC, Singer DS, Mohla S (2017) The Tumor Microenvironment at a Turning Point Knowledge Gained Over the Last Decade, and Challenges and Opportunities Ahead: A White Paper from the NCI TME Network. *Cancer Res* 77: 1051-1059. [Crossref]
14. Quail DF, Joyce JA (2013) Microenvironmental regulation of tumor progression and metastasis. *Nat Med* 19: 1423-1437. [Crossref]
15. Nicolson GL, Dulski KM (1986) Organ specificity of metastatic tumor colonization is related to organ-selective growth properties of malignant cells. *Int J Cancer* 38: 289-294. [Crossref]
16. Raz A, Hanna N, Fidler IJ (1981) In vivo isolation of a metastatic tumor cell variant involving selective and nonadaptive processes. *J Natl Cancer Inst* 66: 183-189. [Crossref]
17. Talmadge JE, Fidler IJ (1982) Cancer metastasis is selective or random depending on the parent tumour population *Nature* 297: 593-594. [Crossref]
18. Fidler IJ (1973) Selection of successive tumour lines for metastasis. *Nature New biology* 242: 148-149. [Crossref]
19. Brunson KW, Nicolson GL.(1978) Selection and biologic properties of malignant variants of a murine lymphosarcoma. *J Natl Cancer Inst* 61: 1499-1503. [Crossref]
20. Fidler IJ (2003) The pathogenesis of cancer metastasis: the 'seed and soil' hypothesis revisited *Nat Rev Cancer* 3: 453-458. [Crossref]
21. Gupta GP, Massague J (2006) Cancer metastasis: building a framework *Cell* 127: 679-695. [Crossref]
22. Kim YS, Yi BR, Kim NH, Choi KC (2014) Role of the epithelial–mesenchymal transition and its effects on embryonic stem cells. *Exp Mol Med* 46: e108. [Crossref]
23. Kim DH, Xing T, Yang Z, Dudek R, Lu Q et al. (2017) Epithelial Mesenchymal Transition in Embryonic Development, Tissue Repair and Cancer: A Comprehensive Overview. *J Clin Med* 7:.[Crossref]
24. Thiery JP, Acloque H, Huang RY, Nieto MA.(2009) Epithelial-mesenchymal transitions in development and disease. *Cell* 139: 871-890. [Crossef]
25. Demirkan B (2013) The Roles of Epithelial-to-Mesenchymal Transition (EMT) and Mesenchymal-to-Epithelial Transition (MET) in Breast Cancer Bone Metastasis: Potential Targets for Prevention and Treatment. *J Clin Med* 2: 264-282. [Crossref]
26. Tsai JH, Yang J (2013) Epithelial-mesenchymal plasticity in carcinoma metastasis. *Genes Dev* 27: 2192-2206. [Crossref]
27. Goldmann WH, Auernheimer V, Thievessen I, Fabry B (2013) Vinculin, cell mechanics and tumour cell invasion. *Cell Biol Int* 37: 397-405. [Crossref]
28. Valvona CJ, Fillmore HL, Nunn PB, Pilkington GJ. (2016) The Regulation and Function of Lactate Dehydrogenase A: Therapeutic Potential in Brain Tumor. *Brain Pathol* 26: 3-17. [Crossref]
29. Facchiano F, Facchiano A, Facchiano AM (2006) The role of transglutaminase-2 and its substrates in human diseases. *Front*

Biosci 11: 1758-1773. [Crossref]

30. Hoskin V, Szeto A, Ghaffari A, Greer PA, Cote GP et al. (2015) Ezrin regulates focal adhesion and invadopodia dynamics by altering calpain activity to promote breast cancer cell invasion. *Mol Biol Cell* 26: 3464-3479. [Crossref]